

Transforming observational data and theoretical isochrones into the ACS/WFC Vega-mag system[†]

Luigi R. Bedin¹^{†‡}, Santi Cassisi², Fiorella Castelli^{3,4}, Giampaolo Piotto¹, Jay Anderson⁵, Maurizio Salaris⁶, Yazan Momany¹, and Adriano Pietrinferni².

¹Dipartimento di Astronomia, Università di Padova, vicolo dell’Osservatorio 2, I-35122 Padova, Italy

²INAF-Osservatorio Astronomico di Collurania, via M. Maggini, 64100 Teramo, Italy

³Istituto di Astrofisica Spaziale e Fisica Cosmica, CNR, via del Fosso del Cavaliere, I-00133 Roma, Italia

⁴INAF-Osservatorio Astronomico di Trieste, via Tiepolo 11, 34131 Trieste, Italia

⁵Department of Physics and Astronomy, Mail Stop 108, Rice University, 6100 Main Street, Houston, TX, 77005, USA

⁶Astrophysics Research Institute, Liverpool John Moores University, 12 Quays House, Birkenhead, CH41 1LD, UK.

Accepted 2004 December 14. Received 2004 May 20; in original form 2004 May 20

ABSTRACT

We propose a zero-point photometric calibration of the data from the ACS/WFC on board the Hubble Space Telescope, based on a spectrum of Vega and the most up to date in-flight transmission curves of the camera. This calibration is accurate at the level of a few hundredths of a magnitude. The main purpose of this effort is to transform the entire set of evolutionary models by Pietrinferni et al. (2004) into a simple observational photometric system for ACS/WFC data, and make them available to the astronomical community. We provide the zero points for the most used ACS/WFC bands, and give basic recipes for calibrating both the observed data and the models.

We also present the Colour Magnitude Diagram (CMD) from ACS data of 5 Galactic globular clusters, spanning the metallicity range $-2.2 < [\text{Fe}/\text{H}] < -0.04$, and provide fiducial points representing their sequences from several magnitudes below the turnoff to the red giant branch tip. The observed sequences are compared with the models in the newly defined photometric system.

Key words: techniques: photometric – stars: imaging – Hertzsprung-Russell (HR) diagram.

1 INTRODUCTION

After two and a half years of operation, the Advanced Camera for Surveys (ACS) on board HST has collected a huge number of observations of stellar systems, and produced a growing database of colour magnitude diagrams (CMDs) and luminosity functions. In order to be able to exploit fully the information contained in these data sets, and to extract a number of fundamental parameters we are interested in, such as metal content, ages, distances, mass functions, etc, we need to compare the observations with theoretical models. The basic requirement for this comparison is the conversion of stellar models into the ACS photometric observational domain. This conversion is the purpose of the present paper. We have

used the most up to date information on the ACS specifications to define a natural, in-flight photometric system and to transform the Pietrinferni et al. (2004) models into the same system. While it is foreseeable that the ACS photometric calibration will improve somewhat as more standard fields are studied and cross compared, the in-flight transmission efficiency curves are now reasonably well established and we would not expect them to change very much. It therefore makes sense to provide a conversion of theoretical stellar models into the observational domain so that more quantitative and qualitative interpretations can be made of observations.

It is worth mentioning that most astronomical photometric investigations are based on some “standard” photometric system. Here, by standard, we mean a photometric system that has been widely used for a long time in different observatories (e.g., the Johnson-Kron-Cousins, Strömgren, Thuan-Gunn, etc systems, see, e.g., Landolt-Börnstein 1982), and possibly defined by a number of standard stars well distributed in the sky, whose flux has been carefully measured. The calibration to a standard system is sometimes the only way to interpret properly the collected data, e.g. when we need to compare our photometric sequences with others collected with different instruments or at different epochs, or with standard results from theoretical models. Still, it must be clearly stated that

[†] Based on observations with the NASA/ESA *Hubble Space Telescope*, obtained at the Space Telescope Science Institute, which is operated by AURA, Inc., under NASA contract NAS 5-26555.

[‡] E-mail: bedin-piotto-momany@pd.astro.it, cassisi-pietrinferni@te.astro.it, castelli@ts.astro.it, jay@eyore.rice.edu, and ms@astro.livjm.ac.uk.

[‡] current address: European Southern Observatory, Karl-Schwarzschild-Str. 2, 85748 b. München, Germany, email: lbedin@eso.org

when the transmission curves of the equipment used to collect the observations are rather different from those of any existing standard system, the transformation of the data to a standard system is difficult, and can be unreliable, particularly for extreme stars (i.e., extreme colours, unusual spectral type, high reddening, etc.).

A good example of a problem that one can encounter in using even slightly different filter sets at the same telescope is given in Momany et al. (2003).

Many of the ACS filters differ substantially from the “standard” filters, and the high photometric precision possible with ACS makes the systematic differences more significant. Thankfully, the filter and instrumental response are better characterized for ACS than they are for the typical ground-based observatory, so that it is possible to avoid standard systems altogether and compare the data and the model in the same system: the observational domain. All that is required for this is to determine an empirical zeropoint for each filter by observing a reference star with a well-characterized spectrum in order to characterize accurately the throughput and response of the detector for each filter. The theoretical models can then be integrated over the same spectral response and compared directly with the data. Such a procedure for comparing models with data is far preferable to the typical procedure of converting both models and data into a “standard” system.

Therefore, we calculated a set of empirical zero points that will allow direct comparison of observational data and theoretical models. We have based our calibration on the reference spectrum of Vega, and so we will refer to our photometric system as the “ACS Vega-mag system”. In our derivation of zero points, we used the in-flight sensitivity, measured by Sirianni et al. (2002, and Sirianni 2003, private communication).

In this paper we have focused our attention on the Wide Field Channel (WFC) of the ACS, but the same procedure can be used to measure the photometric zero points for the High Resolution Channel (HRC).

In the next Section, we describe briefly the total transmission curves, the procedure followed to obtain the zero points, and give the aperture corrections. In Section 3, we briefly describe the adopted stellar evolution models, our procedure to transform the models into the observational plane, and the method used to take into account interstellar absorption. In Section 4 we give the zero points and the formulae to convert both the theoretical tracks and the observed data to the ACS Vega-mag photometric system. Section 5 describes the HST archive data used to test the models, and shows, as an example, how these data have been photometrically calibrated and compared with our models in the ACS Vega-mag plane. Conclusions follow in Section 6 together with instructions on how to download the transformed models.

2 DEFINING THE ACS VEGA-MAG PHOTOMETRIC SYSTEM

In this section, we define our photometric system and will refer to it as the ACS(/WFC) Vega-mag system.

2.1 Total transmission of the HST+WFC/ACS

The first step toward the definition of our photometric system is to calculate the total transmission curves, $T(\lambda)$ for each individual band. These are the products of the individual transmission curves, $t_i(\lambda)$, for 5 different terms.

$$T(\lambda) = t_1(\lambda) \times \dots \times t_5(\lambda)$$

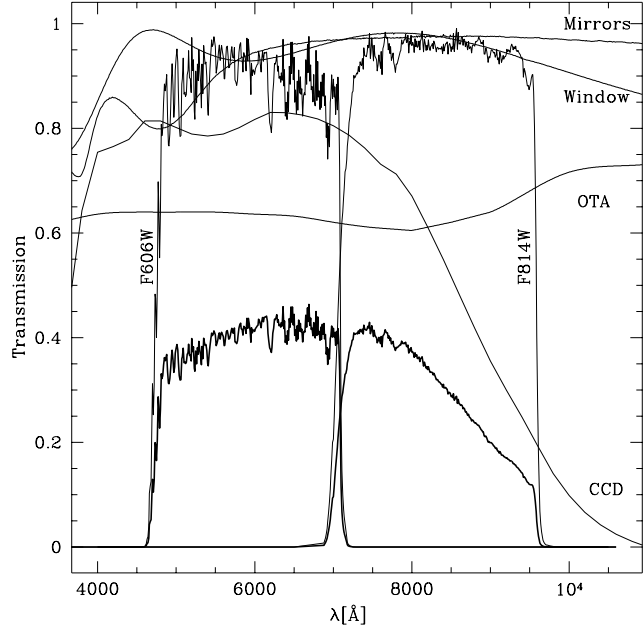


Figure 1. ACS/WFC transmission curves for the window of the dewar, of the WFC/ACS’s Mirrors, of the CCD, of the Optical Telescope Assembly (OTA), and finally the transmission curves for the two ACS/WFC filters: F606W and F814W. The resulting total transmission curve for the two filters is shown as a thick line.

In detail, the $t_i(\lambda)$ are: t_1 the transmission curve of the window of the dewar, t_2 the transmission curve of the filters, t_3 the reflectivity of the WFC/ACS mirrors (3 mirrors), t_4 an average of the two CCD quantum efficiencies¹ and t_5 the transmission curve of the Optical Telescope Assembly (OTA) of HST². In order to outline our procedure, we consider two commonly used filters, F606W and F814W. We will extend the results to other filters in Section 4. All the individual transmission curves are shown in Fig. 1, where two thick lines show the total system transmissions for the two considered filters.

The transmission curves measured in the laboratory differ significantly from those found on-orbit (Sirianni et al. 2002). In the following we will use *only* the on-orbit adjusted total transmission curves obtained by Sirianni et al. (private communication, paper in preparation 2004). The uncertainties for these total transmission curves are within 0.5% (De Marchi et al. 2004³, Sirianni et al. in preparation 2004).

2.2 The Determination of Zero Points

We describe below the procedure used to define the zero points of the system.

We have used the spectrum of Vega from <ftp://ftp.stsci.edu/>

¹ These curves are available at the STSCI web-site http://www.stsci.edu/hst/acs/analysis/reference_files/wfc_synphotable_list.html.

² This last component has been obtained from the web-site <ftp://ftp.stsci.edu/cdbs/cdbs2/comp/ota/> tabulated in the file hst_ota_007_syn.fits.

³ ISR ACS 2004-08, published after the submission of the present work.

cdbs/ cdbs2/ grid/ k93models/ standards/ vega_reference.fits. Details of this spectrum can be found at <http://www.stsci.edu/instruments/observatory/PDF/scs8.rev.pdf>; hereafter it will be denoted as $F^0(\lambda)$, in units $\text{erg s}^{-1}\text{cm}^{-2}\text{\AA}^{-1}$.

The integrated flux of the assumed spectrum of Vega under the total transmission curve T of the filter F606W + instrument is:

$$\begin{aligned}
 I^0(\text{F606W}) &= \int_{-\infty}^{\infty} \dots \simeq \int_{\lambda_{\min}}^{\lambda_{\max}} F^0(\lambda) T_{\text{F606W}}(\lambda) d\lambda = \\
 &= 2.7591 \times 10^{-6} \text{ erg s}^{-1}\text{cm}^{-2}.
 \end{aligned}$$

This number is the quantity that theoreticians will need to rescale their models to the photometric system we adopt (see Sec. 4).

The estimated number of expected photo-electrons (e^-) is:

$$\begin{aligned}
 N_{e^-}^0(\text{F606W}) &= \int_{-\infty}^{\infty} \dots \simeq \int_{\lambda_{\min}}^{\lambda_{\max}} \frac{F^0(\lambda)}{e_{\gamma}(\lambda)} T_{\text{F606W}}(\lambda) d\lambda = \\
 &= 795,861 e^- \text{ s}^{-1}\text{cm}^{-2},
 \end{aligned}$$

where the photon energy $e_{\gamma}(\lambda)$ is given by

$$e_{\gamma}(\lambda) = hc/\lambda \text{ erg.}$$

Therefore, for Vega, the counts detected by the system in digital numbers (DN) would be:

$$\begin{aligned}
 I_{\text{DN}}^0(\text{F606W}) &= N_{e^-}^0(\text{F606W}) \times A_{\text{eff}}/\text{GAIN} = \\
 &= 3.6004 \times 10^{10} / \text{GAIN} \text{ DN s}^{-1},
 \end{aligned}$$

where A_{eff} is the effective collecting area of the telescope (45,239 cm^2 , with the secondary obscuration already accounted for), and GAIN is the conversion factor from e^- to DNs.

At this point, we can define the zero point of our magnitude system in the F606W band by imposing $m_{\text{F606W}} \equiv 0$ for the magnitude of Vega (with the assumed spectrum):

$$Zp^{\text{F606W}} \equiv 2.5 \log_{10} \frac{I_{\text{DN}}^0(\text{F606W})}{[\text{DN s}^{-1}]} = 26.391$$

For simplicity, we have defined this zero point for $\text{GAIN} = 1 \text{ e}^-/\text{DN}$.

Since FLT images provided by STSCI are already in photo-electrons (e^-) rather than in DN (note that DRZ images are given in $\text{e}^- \text{ s}^{-1}$) hereafter, to avoid any confusion, we will not consider the GAIN, and we will refer to I_{e^-} rather than to I_{DN} .

In an analogous way we can define the zero point of the F814W band:

$$Zp^{\text{F814W}} = 25.492,$$

and in a similar way for all the other filters.

2.3 Calibration of the Observations

The formula that observers should use to calibrate their observations into our WFC/ACS Vega-mag system magnitudes in the F606W band is:

$$m_{\text{F606W}} \equiv -2.5 \log_{10} \frac{I_{e^-}}{\text{exptime}} + Zp^{\text{F606W}} - Z_{\text{Aperture}}$$

where exptime is the exposure time, and Z_{Aperture} is the aperture correction. In the next section we discuss in detail the aperture correction, which we will always treat as a positive quantity to be

FILTER	$\Delta m_{\text{AP}(\infty)-\text{AP}(\infty)}$	$\Delta m_{\text{AP}(0''.5)-\text{AP}(\infty)}$	$\Delta m_{\text{AP}(0''.3)-\text{AP}(\infty)}$
F435W	0.000	0.095	0.132
F475W	0.000	0.084	0.120
F502N	0.000	0.078	0.114
F550M	0.000	0.076	0.110
F555W	0.000	0.076	0.110
F606W	0.000	0.079	0.115
F625W	0.000	0.080	0.118
F658N	0.000	0.079	0.123
F660N	0.000	0.079	0.123
F775W	0.000	0.078	0.123
F814W	0.000	0.079	0.130

Table 1. $\Delta m_{\text{AP}(r)-\text{AP}(\infty)}$ corrections to be added to the Zero Points.

subtracted. This calibration is intended for the officially calibrated DRZ images which are already corrected for: flat field, dark, bias, and geometrical distortion.⁴

2.4 Aperture Corrections

Breathing of the telescope tube, the complex optical system, and charge diffusion induce temporal and spatial variation of the core of the point-spread function (PSF), such that the 1st-ring ratio of the diffraction figure changes considerably across the chip and at a minor level with orbital phase.

For these reasons, we choose to refer our zero points to an infinite aperture. That makes it easier for those studying surface photometry of extended sources to calibrate their magnitudes to this system. The aperture corrections for extended sources are null, being the Zero Points of the system referred to an infinite aperture.⁵

$$Z_{\text{Aperture}} = 0.$$

On the other hand, in practice all the energy of a point source is contained within 4'' (~ 80 pixels), and $\sim 93\%$ within 0.''5 (~ 10 pixels). In dense environments, where crowding makes an aperture correction to an infinite aperture impossible, one has to rely on the in-flight encircled energy.⁶ This means that one has to correct the instrumental magnitude (for example the PSF-fitted magnitude) to the magnitude at a specified aperture r by adding a $\Delta m_{\text{PSF}-\text{AP}(r)}$, and then sum an additional quantity $\Delta m_{\text{AP}(r)-\text{AP}(\infty)}$, obtained from the tabulated encircled energy in order to link the magnitudes to the infinite aperture for which we have calculated the Zero Points.

In summary,

$$Z_{\text{Aperture}} = \Delta m_{\text{PSF}-\text{AP}(r)} + \Delta m_{\text{AP}(r)-\text{AP}(\infty)}.$$

In Table 1 we give the $\Delta m_{\text{AP}(r)-\text{AP}(\infty)}$ corrections to be added to the zero points for two circular apertures of radius 0.''3 (~ 6 pixels) and 0.''5 (as in Holtzman et al. 1995) and for the different filters. For clarity, we also report in Tab. 1 the correction to zero points for an infinite aperture, which is zero by definition.

For point sources, the $\Delta m_{\text{PSF}-\text{AP}(r)}$ correction should be estimated in each individual image, remembering that the smaller the

⁴ The images are still affected, at least by CTE, and charge diffusion (see Riess & Mack, ISR 2004-06, and Krist, ISR 2003-06). In Section 5.1 we use FLT images, and describe how we linked our photometry for those images to the officially corrected DRZ images.

⁵ Note, that this is really only true for infinite extended sources, or sources larger than the widest part of the PSF halo.

⁶ This is tabulated at the STSCI web-site: http://www.stsci.edu/hst/acs/analysis/reference_files/wfc_synphottable_list.html

aperture (r), the more the photometry is affected by the problems mentioned at the beginning of this section (i.e. spatial variability of the PSF and charge diffusion). See Section 5.2 for uncertainties on the values of $\Delta m_{\text{PSF-AP}(r)}$.

Moreover, there appears to be a second-order effect which depends on the colour of the stars and on the filter used (Sirianni, private communication, paper in preparation). In practice, the present calibration is useful only if the degree of accuracy desired by the observers is no better than 2-3 hundredths of a magnitude. However, taking into account all the problems of ACS, it seems hard to achieve a much higher accuracy. It should be noted that the photometric stability of WFPC2 was certainly not any better than this, but the higher precision of WFC/ACS makes systematic errors (on the zero points) the dominant source of error in the final photometry.

We have decided not to deal with the two filters: F850LP and F892N, because they are much more problematic (see Sirianni, in preparation).

3 TRANSFORMING THE STELLAR MODELS INTO THE ACS VEGA-MAG SYSTEM

3.1 The Stellar Evolution Models

In this work we adopt the stellar-evolution model database in Pietrinferni et al. (2004); for a detailed description of the models, as well as a comparison with other stellar model libraries available in the literature, we refer the interested reader to this reference. For the purposes of this paper, we briefly list the main characteristics of this model library.

Evolutionary tracks are available for up to 41 mass values at each of 10 selected initial chemical compositions. The minimum mass considered is roughly $0.5M_{\odot}$, while the maximum value is always equal to $10M_{\odot}$. The whole set of evolutionary computations has been used to compute isochrones for a large age range, from ~ 40 Myr to ~ 14 Gyr, covering all stellar evolution phases from the Zero Age Main Sequence up to the first thermal pulse on the Asymptotic Giant Branch or to C ignition. For each chemical composition, a Zero Age Horizontal Branch (ZAHB) locus, as well as post-ZAHB evolutionary tracks were also calculated for a large range of masses, by employing the He-core mass and chemical profiles in the H-rich envelope of the Red Giant Branch (RGB) progenitor having an age at the He-flash of the order of $\sim 12 - 13$ Gyr.

The set of models has been computed for metallicities in the range $0.0001 \leq Z \leq 0.04$ for both a scaled-solar mixture and an α -enhanced mixture ($\langle [\alpha/\text{Fe}] \rangle = 0.4$; paper in preparation).

The adopted reference scaled-solar heavy element mixture is from Grevesse & Noels (1993). As for the He-abundance, the models employ a primordial mass fraction of $Y_0 = 0.245$, based on the estimates by Cassisi et al. (2003, see also Salaris et al. 2004) obtained from the R -parameter method applied to a large sample of Galactic globular clusters (GGCs). This Y_0 value is in fair agreement with recent independent determinations of the cosmological baryon density from the WMAP results (Spergel et al. 2003). To reproduce the initial solar He-abundance obtained from an appropriately calibrated solar model, an He enrichment ratio $dY/dZ = 1.4$ has been used (Pietrinferni et al. 2004).

All models have been computed with outer boundary conditions obtained by integrating the atmospheric layers with the Krishna-Swamy (1966) $T(\tau)$ relationship. Superadiabatic convection is treated according to the Cox & Giuli (1968) formalism of

mixing-length theory (Böhm-Vitense 1958), and the mixing-length parameter has been fixed by the solar calibration ($ml = 1.713$) and kept constant for all masses during all evolutionary phases; mass loss is included by employing the Reimers formula (Reimers 1975) with the free parameter η set to 0.4.

At each chemical composition, models have been computed with and without overshooting from the convective cores during the main sequence (MS) phase. In the former case, $\lambda_{OV} = 0.20 \times H_P$ for masses larger than $1.7M_{\odot}$, where λ_{OV} is the extension of the overshooting region in units of the local pressure scale height. For stars less massive than $1.1M_{\odot}$, $\lambda_{OV} = 0$, while in the intermediate range λ_{OV} varies according to the relation $\lambda_{OV} = (M/M_{\odot} - 0.9)/4$. This choice allows a smooth variation of the isochrone turn-off (TO) morphology, and a smooth decrease to zero of the convective core mass. This parametrization also provides a good match to the TO morphology in the CMD of Galactic open clusters of different ages. Induced overshooting and semi-convection during the central He-burning phase are accounted for following Castellani et al. (1985).

Radiative opacities from the OPAL tables (Iglesias & Rogers 1996) for temperatures larger than 10^4 K, and from Alexander & Ferguson (1994) for lower temperatures have been employed, supplemented by opacities for electron degenerate matter computed following Potekhin (1999). The relevant energy loss rate from plasma-neutrino processes comes from Haft, Raffelt & Weiss (1994), whereas for all other processes the reader is referred to Cassisi & Salaris (1997); the nuclear reaction rates are from the NACRE database (Angulo et al. 1999), with the exception of the $^{12}\text{C}(\alpha, \gamma)^{16}\text{O}$ reaction, in which case the more accurate recent determination by Kunz et al. (2002) has been adopted. Electron screening is treated according to Graboske et al. (1973).

The accurate Equation of State (EOS) by A. Irwin has been used. An exhaustive description of this EOS is in preparation (Irwin et al. 2004) but a brief discussion of its main characteristics can be found in Cassisi et al. (2003). This EOS covers the full stellar structure for the whole evolutionary phase and mass range spanned by the model database; in Pietrinferni et al. (2004) and Bahcall, Serenelli & Pinsonneault (2004) it is shown that this EOS and the latest version of the OPAL EOS (Rogers 2001) provide almost identical results in the case of the Sun. The accuracy and reliability of the present evolutionary scenario has been successfully tested in Cassisi et al. (2003), Riello et al. (2003) and Salaris et al. (2004) in the regime of Galactic globular clusters, and by Pietrinferni et al. (2004) in the regime of field stars and open clusters. Cassisi et al. (2003) and Pietrinferni et al. (2004) have also compared our adopted set of theoretical isochrones with other existing isochrone databases widely cited in the current literature. This comparison provides an estimate of the present uncertainties in stellar evolution models due to different choices for the stellar input physics (see also Chaboyer 1995). The main conclusions of this exercise are summarized below.

Isochrones for typical globular cluster ages (of the order of 10 Gyr) show a remarkable consistency for the prediction of the Main Sequence location and Turn Off luminosity at a given initial chemical composition, whereas the Red Giant Branch effective temperature and Zero Age Horizontal Branch brightness display values that differ by amounts of $\sim 100-200$ K and ~ 0.1 mag, respectively. Globular cluster ages estimated from the difference between Turn Off and Horizontal Branch brightness would consequently be uncertain by ~ 10 % (Chaboyer 1995 determined a similar uncertainty, of the order of 15%).

Isochrones for ages lower than $\sim 4-5$ Gyr show again consistent Main Sequence locations, but differing Turn Off luminosi-

ties, effective temperatures, and Helium burning luminosities, due mainly to the uncertain treatment of the overshooting from the Main Sequence stars' convective cores. These uncertainties cause variations in the estimated age of stellar populations within this age range, of at most $\sim 30\%$. Also in this age range red giants' effective temperatures show a spread of $\sim 100\text{--}200$ K.

3.2 The Transformation to the Observational Plane

Here we describe the procedure we have followed to transform our models into the ACS Vega-mag system defined in Sect. 2.

We computed ACS colour indices by using the homogeneous set of ODFNEW model atmospheres and synthetic fluxes⁷ (Castelli & Kurucz 2003) computed with the Kurucz ATLAS9 code. We generated grids of indices for the following values of [Fe/H]: 0.5, 0.2, 0.0, -0.5 , -1.0 , -1.5 , -2.0 , -2.5 .

In each grid point, T_{eff} ranges from 3500 to 50,000 K, $\log g$ from 0.0 to 5.0 and the microturbulent velocity is $\xi=2.0$ km s $^{-1}$. We tabulated for each T_{eff} and $\log g$ gridpoint the BC_V bolometric correction, the V magnitude, and the colour indices $V - m_{\text{F435W}}$, $V - m_{\text{F475W}}$, $V - m_{\text{F555W}}$, $V - m_{\text{F606W}}$, $V - m_{\text{F625W}}$, $V - m_{\text{F775W}}$, and $V - m_{\text{F814W}}$. The ACS magnitudes were computed by using the WFC/ACS transmission curves described in Sect. 2.1, while we adopted the V passband from Bessel (1990).

We adopted $V = 0.03$ for Vega and set all colour indices ($V - m_{\text{filter}}^{\text{ACS}}$) to zero, so that the Vega ACS magnitudes would be equal to 0.00 in all passbands. The Vega model and flux are the ATLAS9 model and the ATLAS9 flux from Castelli & Kurucz (1994) with parameters $T_{\text{eff}}=9550$ K, $\log g=3.95$, $[\text{M}/\text{H}]=-0.5$, $\xi=2$ km s $^{-1}$. Note that this model has been built specifically to reproduce the observations of the spectrum used in Sect. 2.2. The absolute zero-point for the V magnitude was fixed by adding the constant -21.10 mag to the computed V for Vega (Bessell, Castelli & Plez 1998).

In Table 2 we show an example of the theoretical isochrones transformed into the ACS Vega-mag photometric system. The header of the isochrone table provides information about the number of lines in the file (N_P), the total metallicity [M/H], the abundance by mass of metals (Z) and helium (Y), and the corresponding age in billions of years, $t(\text{Gyr})$. The content of the columns in the following lines is the following (from left to right): 1) the initial mass of each star, 2) the current mass at the specified age (computed accounting for mass loss - see previous section), 3) the logarithm of the surface luminosity in solar units, 4) the logarithm of the effective temperature, 5) the ACS M_{F435W} magnitude, 6) the ACS M_{F475W} magnitude, 7) the ACS M_{F555W} magnitude, 8) the ACS M_{F606W} magnitude, 9) the ACS M_{F625W} magnitude, 10) the ACS M_{F775W} magnitude, 11) the ACS M_{F814W} magnitude.

The entire set of transformed isochrones, as well as the ZAHB and post-ZAHB evolutionary tracks can be retrieved from the following URL: <http://www.te.astro.it/BASTI/index.php>.

3.3 Reddening in the WFC/ACS Vega-mag system

Following the recipe and the motivations given by Holtzman et al. (1995) we also computed the interstellar absorption in the WFC/ACS bands as a function of $E(B-V)$. By using the extinction curve from Table 1 in Mathis (1990) for $R_V = 3.1$ we computed for different values of $E(B-V)$ the interstellar reddening A_{λ} at the wavelengths of the ATLAS9 flux, the corresponding reddened

fluxes and the reddened WFC/ACS magnitudes. The A_{filter} extinctions in the WFC/ACS filters were obtained as differences between the reddened and unreddened m_{filter} magnitudes.

Tables 3 and 4 give the values of the A_{filter} for a cool star and a hot star respectively. We give these values for the main filters, F435W, F475W, F555W, F606W, F625W, F775W, and F814W. We note how these values are very close to those tabulated by Holtzman et al. (1995) for WFPC2's similar filters.

4 ACS VEGA-MAG SYSTEM ZERO POINTS

Table 5 lists the zero points for the ACS Vega-mag system in other useful pass-bands; the zero points for all the other filters can be easily obtained following the recipes outlined above.

We note that this calibration is linked to the chosen spectrum of Vega. These zero points are probably accurate to 2–3 hundredths of a magnitude, and can (and hopefully will soon) be updated, once more accurate data on the ACS performance is available.

The main sources of systematic error in the calibration of the observations are: residuals in correction for CTE, flat fielding, aperture corrections, charge diffusion, and the encircled energy which seems to depend on stellar colour (Sirianni, private communication). Still, the lack of any other official and complete photometric calibration of the ACS, useful for the comparison with stellar models, has led us to calculate and publish this calibration.

In summary, photometric observations can be transformed into the ACS/WFC Vega-mag system defined in this paper by applying the following relation:

$$m_{\text{filter}} \equiv -2.5 \log_{10} \frac{I_{\text{e}^-}}{\text{exptime}} + Zp^{\text{filter}} + \\ - \Delta m_{\text{PSF-AP}(r)}^{\text{filter}} - \Delta m_{\text{AP}(r)-\text{AP}(\infty)}^{\text{filter}}; \quad (1)$$

Where r can assume the values: ∞ , $0''.5$, or $0''.3$. Note that the last two positive quantities in Eq. 1 are subtracted.

Models can be transformed into the observational plane of the same system by applying:

$$M_{\text{filter}} = -2.5 \log_{10} \frac{I(\text{filter})}{I^0(\text{filter})}. \quad (2)$$

Here the meaning of $I(\text{filter})$, and $I^0(\text{filter})$ are clear from the discussions in previous sections. In Sect. 5.2 we give a practical example of how to calibrate the observations.

Our Zero points agree well with those presented in the recent ISR by De Marchi et al. (2004–08).⁸ The only differences are due to a different choice of spectrum of Vega (Sirianni private communication). Nevertheless, for broad filters the Zero points agree within ~ 0.005 mag.

5 COMPARISON OF MODELS WITH OBSERVATIONS

5.1 Observations and Data Reduction

In order to give a practical example of our procedures and to provide a useful test for our models, we used archival WFC observations of 5 Galactic globular clusters (GO-9453, PI: Brown), which span a wide range in metallicity ($-2.2 < [\text{Fe}/\text{H}] < -0.04$). The

⁷ Available at <http://wwwuser.oat.ts.astro.it/castelli/grids.html>.

⁸ <http://www.stsci.edu/hst/acs/documents/isrs/isr0408.pdf>.

Isochrone by Pietrinferni - Cassisi - Salaris - Castelli 2004 Standard Model
 Scaled solar model & transformations for ACS (Castelli 2004)

$Np = 2000$, $[M/H] = -0.659$, $Z = 0.0040$, $Y = 0.251$, $t(Gyr) = 11.0000$

$(M/M_{\odot})_{\text{in}}$	(M/M_{\odot})	$\log L/L_{\odot}$	$\log T_{\text{eff}}$	M_{F435W}	M_{F475W}	M_{F555W}	M_{F606W}	M_{F625W}	M_{F775W}	M_{F814W}
.5000000000	.4999030025	-1.20676	3.62790	9.540	9.063	8.418	8.024	7.693	7.069	6.982
.5011654487	.5011233468	-1.20259	3.62829	9.525	9.048	8.405	8.012	7.681	7.059	6.972
.502308974	.5023308974	-1.19841	3.62868	9.510	9.034	8.392	8.000	7.670	7.049	6.962
...
.9066248329	.6047402926	2.89310	3.60793	-0.175	-0.871	-1.635	-2.045	-2.382	-3.053	-3.153
.9066266265	.6037663031	2.92275	3.60503	-0.190	-0.899	-1.675	-2.093	-2.435	-3.116	-3.218
.9066284200	.6026715201	2.95336	3.60202	-0.204	-0.926	-1.715	-2.143	-2.490	-3.181	-3.285

Table 2. Example of an isochrone available at <http://www.te.astro.it/BASTI/index.php>.

$T_{\text{eff}} = 4,000\text{K}$, $\log g = 4.50$, $[M] = 0.00$, $v_{\text{turb}} = 2.00$, $l/H = 1.25$							
$E(B-V)$	A_{F435W}	A_{F475W}	A_{F555W}	A_{F606W}	A_{F625W}	A_{F775W}	A_{F814W}
0.00	0.000	0.000	0.000	0.000	0.000	0.000	0.000
0.05	0.202	0.182	0.158	0.140	0.132	0.099	0.092
0.10	0.404	0.365	0.316	0.279	0.263	0.198	0.184
0.15	0.606	0.546	0.474	0.419	0.394	0.297	0.276
0.20	0.808	0.728	0.632	0.558	0.526	0.396	0.367
0.25	1.010	0.909	0.790	0.696	0.657	0.495	0.459
0.30	1.212	1.090	0.947	0.834	0.788	0.594	0.550
0.35	1.413	1.271	1.104	0.972	0.919	0.692	0.641
0.40	1.614	1.451	1.262	1.110	1.050	0.791	0.732
0.45	1.815	1.631	1.419	1.248	1.180	0.890	0.823
0.50	2.017	1.811	1.575	1.385	1.311	0.988	0.913
0.55	2.217	1.990	1.732	1.522	1.442	1.086	1.004
0.60	2.418	2.169	1.889	1.658	1.572	1.185	1.094
0.65	2.619	2.348	2.045	1.794	1.702	1.283	1.184
0.70	2.819	2.527	2.201	1.930	1.833	1.381	1.274
0.75	3.020	2.705	2.357	2.066	1.963	1.479	1.364
0.80	3.220	2.883	2.513	2.202	2.093	1.577	1.454
1.00	4.020	3.592	3.136	2.741	2.612	1.968	1.811
1.25	5.016	4.472	3.911	3.409	3.260	2.454	2.254
1.50	6.010	5.347	4.682	4.072	3.905	2.939	2.693
1.75	7.001	6.215	5.450	4.730	4.547	3.422	3.128
2.00	7.990	7.077	6.216	5.382	5.188	3.902	3.559
2.25	8.975	7.935	6.978	6.031	5.827	4.381	3.987
2.50	9.959	8.788	7.737	6.675	6.463	4.858	4.411
2.75	10.940	9.636	8.494	7.315	7.098	5.333	4.832
3.00	11.919	10.480	9.249	7.951	7.731	5.806	5.250
3.25	12.896	11.320	10.001	8.585	8.362	6.277	5.664
3.50	13.871	12.157	10.751	9.215	8.991	6.747	6.075
3.75	14.844	12.991	11.499	9.843	9.619	7.215	6.483
4.00	15.815	13.822	12.244	10.468	10.245	7.681	6.888
4.25	16.785	14.650	12.988	11.091	10.870	8.145	7.291
4.50	17.753	15.476	13.730	11.711	11.493	8.608	7.690
4.75	18.719	16.299	14.470	12.329	12.115	9.070	8.088
5.00	19.684	17.120	15.209	12.946	12.735	9.530	8.483

Table 3. Extinctions (in mag) in different ACS filters as a function of the colour excess $E(B-V)$ of a cool star.

$E(B-V)$	A_{F435W}	A_{F475W}	A_{F555W}	A_{F606W}	A_{F625W}	A_{F775W}	A_{F814W}
0.00	0.000	0.000	0.000	0.000	0.000	0.000	0.000
0.05	0.212	0.194	0.165	0.153	0.135	0.102	0.096
0.10	0.423	0.387	0.329	0.305	0.269	0.203	0.192
0.15	0.635	0.580	0.493	0.456	0.403	0.304	0.288
0.20	0.846	0.773	0.657	0.608	0.538	0.406	0.383
0.25	1.057	0.965	0.821	0.759	0.672	0.507	0.479
0.30	1.267	1.157	0.985	0.909	0.806	0.608	0.574
0.35	1.478	1.348	1.148	1.059	0.940	0.709	0.669
0.40	1.688	1.539	1.311	1.209	1.073	0.810	0.764
0.45	1.898	1.730	1.474	1.358	1.207	0.911	0.859
0.50	2.108	1.921	1.637	1.507	1.341	1.012	0.953
0.55	2.318	2.111	1.800	1.656	1.474	1.112	1.048
0.60	2.527	2.300	1.963	1.804	1.608	1.213	1.142
0.65	2.737	2.490	2.125	1.951	1.741	1.313	1.237
0.70	2.946	2.678	2.288	2.099	1.874	1.414	1.331
0.75	3.155	2.867	2.450	2.246	2.007	1.514	1.424
0.80	3.364	3.055	2.612	2.392	2.140	1.615	1.518
1.00	4.196	3.804	3.258	2.975	2.671	2.015	1.891
1.25	5.233	4.732	4.062	3.694	3.333	2.513	2.354
1.50	6.265	5.651	4.862	4.405	3.992	3.009	2.813
1.75	7.292	6.562	5.658	5.107	4.648	3.503	3.268
2.00	8.315	7.465	6.450	5.800	5.302	3.995	3.719
2.25	9.333	8.360	7.239	6.486	5.954	4.485	4.166
2.50	10.347	9.247	8.023	7.165	6.603	4.972	4.609
2.75	11.357	10.128	8.804	7.837	7.250	5.458	5.048
3.00	12.362	11.003	9.581	8.503	7.895	5.942	5.483
3.25	13.364	11.872	10.355	9.163	8.538	6.423	5.915
3.50	14.362	12.735	11.126	9.818	9.178	6.902	6.343
3.75	15.357	13.594	11.894	10.468	9.817	7.380	6.767
4.00	16.348	14.447	12.658	11.114	10.453	7.856	7.187
4.25	17.336	15.297	13.420	11.755	11.088	8.329	7.604
4.50	18.321	16.142	14.179	12.393	11.721	8.801	8.018
4.75	19.303	16.985	14.935	13.028	12.352	9.271	8.429
5.00	20.283	17.823	15.689	13.659	12.981	9.740	8.837

Table 4. As in Table 3, but for a hot star.

filter	F435W	F475W	F502N	F550M	F555W	F606W
$Zp_{\text{filter}}^{\text{filter}}$	25.785	26.168	22.338	24.861	25.718	26.391
$I^0(\text{filter})$	2.0994	2.7611	0.075320	0.69396	1.6028	2.7591
filter	F625W	F658N	F660N	F775W	F814W	—
$Zp_{\text{filter}}^{\text{filter}}$	25.722	22.381	21.342	25.254	25.492	—
$I^0(\text{filter})$	1.3687	0.059770	0.022895	0.72740	0.87198	—

Table 5. Natural ACS-VEGA System Zero Points ($Zp_{\text{filter}}^{\text{filter}}$), and Fluxes $I^0(\text{filter})$ (in $10^{-6} \text{ erg s}^{-1} \text{ cm}^{-2}$).

data are summarized in Table 6. They consist of 1 short, 1 intermediate, and 1 (relatively) long exposure, in both F606W and F814W filters, for each cluster.

We carried out the photometry with algorithms based on the effective point-spread function (ePSF) fitting procedure described by Anderson & King (2000). We obtained the ePSF from a set of images from a different project using the same filters, since the dithering of GO-9453 images was unsuitable to constrain the ePSF shape (Anderson & King, 2000).

The resampling present in the DRZ images provided by STSCI does not allow the use of the ePSF method, limiting the precision of the output photometry. We therefore performed our fitting photometry using FLT images. These images, affected by geometrical distortion, have been flat-fielded to preserve surface brightness, but not flux. Therefore, we must multiply each pixel by its projected area to obtain a proper flux for each star.

We find slight differences of flux-scaling between our corrected FLT images and the corresponding DRZ images (on the order of 1% or so). Since it is the DRZ images that have been carefully calibrated via the STSCI pipe-line, we should convert any photometry measured on FLT images into the corresponding infinite-aperture fluxes in the DRZ images. The photometry has been calibrated as described in the previous sections.

5.2 An Example: Calibration of the 47Tuc Photometry

For the GO-9453 47Tuc data, the zero point of the long exposures has been used to calibrate the intermediate and short ones in both F606W (for which the exposure time is 70s) and F814W filters (for which the exposure time is 72s, see Table 3). We determined the zero-point difference between our PSF-fitting photometry and aperture photometry with a $0''.5$ aperture for each filter. The differences are $\Delta m_{\text{PSF-AP}(0''.5)}^{\text{F606W}} = +0.15(\pm 0.015)$, and $\Delta m_{\text{PSF-AP}(0''.5)}^{\text{F814W}} = +0.25(\pm 0.015)$. To these we need to add the aperture corrections. According to Table 1: $\Delta m_{\text{AP}(0''.5)-\text{AP}(\infty)}^{\text{F606W}} = \Delta m_{\text{AP}(0''.5)-\text{AP}(\infty)}^{\text{F814W}} = +0.079$ (equal for the two filters, at this apertures). In summary, from Eq. (1):

$$m_{\text{F606W}} \equiv -2.5 \log_{10} \frac{I_{\text{e}}^-}{70} + 26.391 - 0.15 - 0.079$$

$$m_{\text{F814W}} \equiv -2.5 \log_{10} \frac{I_{\text{e}}^-}{72} + 25.492 - 0.25 - 0.079$$

[Note: 1) $-2.5 \log_{10} I_{\text{e}}^-$ is simply the instrumental magnitude (some codes, such as DAOPHOT, add a constant value of 25 to the instrumental magnitude to avoid negative numbers); 2) the adopted normalization of the fitting magnitude is taken into account by the aperture correction $\Delta m_{\text{PSF-AP}(r)}$; 3) the sign of the last two quantities in each equation is negative.]

The calibrated CMDs are presented in Fig. 2. Superposed on

Cluster	F606W data	F814W data
NGC 6528	4s, 50s, 450s	1s, 20s, 350s
NGC 5927	2s, 30s, 500s	0.7s, 15s, 340s
NGC 104	0.5s, 6s, 70s	0.5s, 5.5s, 72s
NGC 6752	0.5s, 4s, 40s	0.5s, 4s, 45s
NGC 6341	0.5s, 5s, 90s	0.5s, 6s, 100s

Table 6. Data set of the observed clusters.

the observed CMD are the fiducial lines of the MS, SGB, and RGB. The fiducial points which define them have been determined by eye and are given in Table 7. Note that, due to the differential reddening in the field, the fiducial lines in the cases of NGC 6528 and NGC 5927 are poorly defined.

These fiducial points can be used as a reference to compare against those measured for other globular clusters or galaxies whose stars are resolved (Brown et al. 2003).

5.3 Comparison with the Models

In this section we compare the theoretical models transformed to the ACS Vega-mag system with observed CMDs.

Figure 3 displays our adopted α -enhanced isochrones and ZAHBs compared with the observed CMDs of the GGCs 47 Tuc (NGC 104), NGC 6752, and M92 (NGC 6341). These clusters span a wide metallicity range ($-2.2 < [\text{Fe}/\text{H}] < -0.6$). We selected these clusters for the comparison because of their very low extinction and lack of differential reddening.

In the following discussion, in order to make the comparison with the values in the literature more straightforward, we give the reddening $E(B-V)$ and the apparent distance modulus in the V band (y_V). The $E(B-V)$ comes from $E(m_{\text{F606W}} - m_{\text{F814W}}) = A_{\text{F606W}} - A_{\text{F814W}}$ as adopted in the best fitting by interpolation of the values in Table 3. The y_V comes from the best fitting distance modulus in the F606W band (y_{F606W}): $y_V = y_{\text{F606W}} - A_{\text{F606W}} + A_V$, where $A_V = 3.1E(B-V)$.

In the case of 47 Tuc we used α -enhanced ($<[\alpha/\text{Fe}]> = 0.4$) isochrones with $[\text{Fe}/\text{H}] = -0.66$ ($Z = 0.008$), a value in very good agreement with spectroscopic measurements (see, e.g., Percival et al. 2002, Gratton et al. 2003); the best match is obtained for an apparent distance modulus $y_V = 13.45$, an age of 10 Gyr, and a reddening $E(B-V) = 0.04$ (the 8 and 13 Gyr isochrones are also shown). These values of distance modulus and reddening are consistent with empirical determinations by Percival et al. (2002) and Gratton et al. (2003).

The quality of the fit is satisfactory along most of the isochrone, worsening at the redder end of both the RGB and MS. The deviation of the lower part of the sequence from the models for intermediate-metallicity clusters is well known (see Bedin et al. 2001).

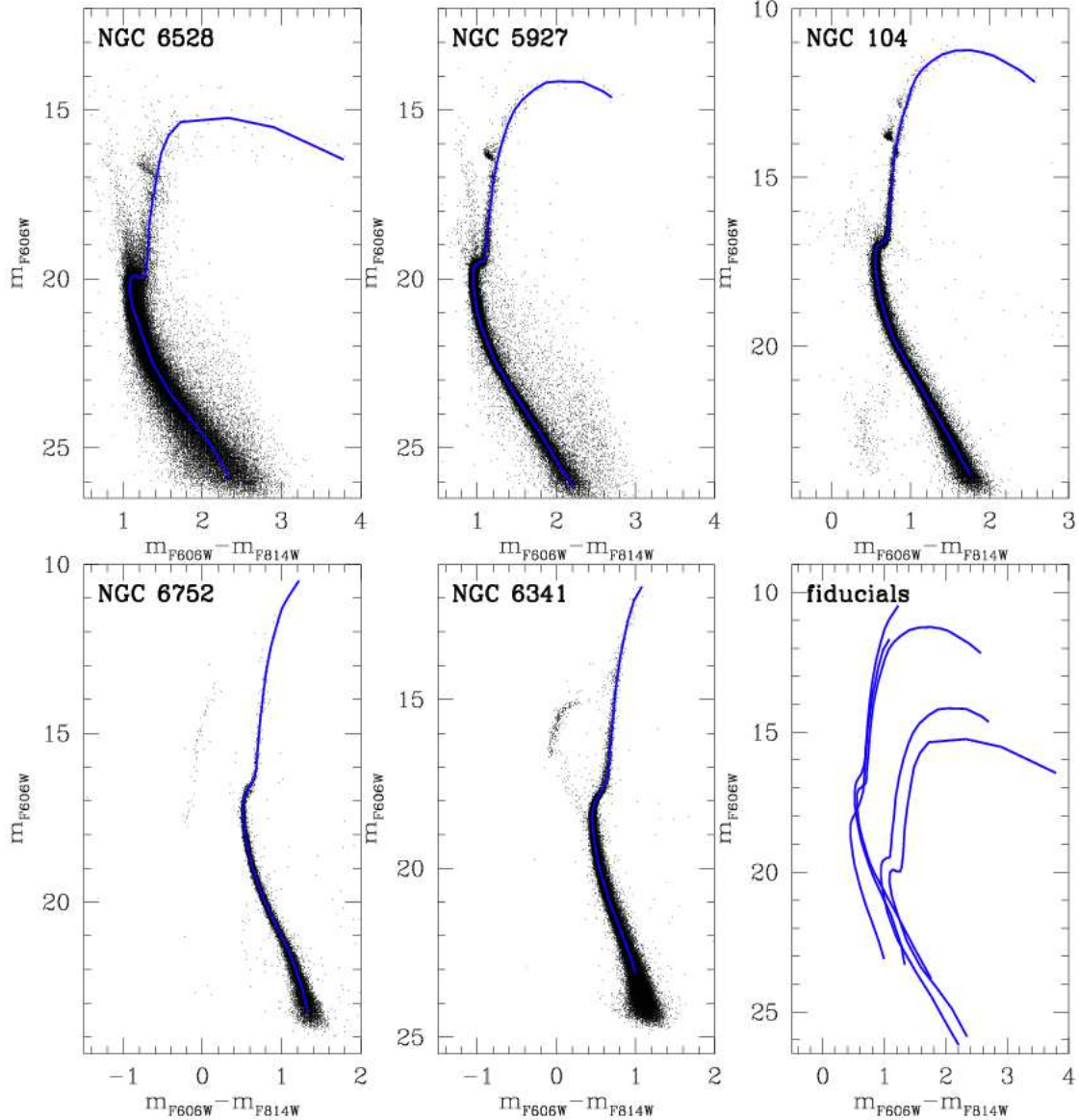


Figure 2. Observed CMDs for the five clusters discussed in the text and summarized in Tab. 6. The fiducials are overplotted onto each CMD, and shown together in the bottom-right panel for comparison.

For NGC 6752 we have employed our isochrones with $[\text{Fe}/\text{H}] = -1.26$ ($Z=0.002$), a value close to the estimate by Rutledge et al. (1997) with their calibration of the CaII triplet index on the GGC Carretta & Gratton (1997) metallicity scale. We obtain a best match with $y_V=13.25$, an age of 12 Gyr and $E(B-V)=0.04$ (the 10 and 14 Gyr isochrones are also shown).

Again, the reddening agrees with independent empirical estimates (e.g. Gratton et al. 2003), whereas the distance is slightly longer than the MS-fitting estimates (Carretta et al. 2000, Gratton et al. 2003). These empirical estimates employ a metallicity ~ 0.2 dex lower than our adopted value; it is interesting to note, judging from the numerical experiment performed by Carretta et al. (2000, their Fig. 5), that their empirical MS-fitting distance would come into agreement with our value if our assumed metallicity is used in their MS-fitting technique.

Had we used our isochrones for $[\text{Fe}/\text{H}] = -1.57$ ($Z=0.001$)

and a value close to the metallicity estimate by Rutledge et al. (1997) obtained calibrating the calcium index on the Zinn & West (1984) metallicity scale, the quality of the fit to the RGB location would be worse (isochrone too blue), the age older by ~ 1 Gyr, $E(B-V) \sim 0.02$ mag higher and $y_V \sim 0.07$ mag larger.

The comparison with the M 92 (NGC 6341) CMD has been performed using isochrones with $[\text{Fe}/\text{H}] \approx -2.1$ ($Z=0.0003$), a value in fair agreement with the estimate by Carretta & Gratton (1997) ($[\text{Fe}/\text{H}] = -2.16$). The best agreement is achieved for an age of 12 Gyr, $E(B-V)=0.04$ and $y_V = 14.85$ (the 10 and 14 Gyr isochrones are also shown).

6 SUMMARY

In this paper we have proposed a simple zero-point photometric calibration of the ACS/WFC data, based on a model spectrum of Vega

		NGC 104		NGC 6341	
		Colour	Mag	Colour	Mag
NGC 5927		2.57	12.17	1.08	11.67
		2.38	11.83	0.98	12.06
Colour	Mag	2.05	11.39	0.90	12.70
		1.92	11.30	0.80	13.73
NGC 5928		1.75	11.23	0.74	14.77
		2.70	14.63	1.22	10.48
Colour	Mag	2.59	14.45	1.08	10.99
		2.33	14.17	1.00	11.32
NGC 5928		1.40	11.36	0.94	11.80
		2.03	14.15	1.27	11.55
Colour	Mag	1.87	14.18	1.16	11.78
		1.72	14.38	1.07	12.03
NGC 5928		1.57	14.69	1.01	12.35
		2.33	15.24	1.56	11.25
Colour	Mag	1.46	15.02	0.94	12.84
		1.72	15.36	0.88	13.32
NGC 5928		1.39	15.40	0.73	14.60
		1.57	15.75	0.71	15.10
Colour	Mag	1.31	15.93	0.69	15.60
		1.48	16.26	0.80	14.26
NGC 5928		1.24	16.59	0.68	15.91
		1.43	16.85	1.18	17.18
Colour	Mag	1.18	17.18	0.76	14.90
		1.38	17.59	0.74	15.55
NGC 5928		1.15	17.84	0.73	15.98
		1.33	18.41	1.12	18.53
Colour	Mag	1.01	19.33	0.71	18.94
		1.28	19.82	1.11	19.21
NGC 5928		1.26	19.97	1.10	19.32
		1.20	19.97	1.08	19.44
Colour	Mag	1.14	19.89	0.69	16.81
		1.09	20.02	0.67	16.90
NGC 5928		1.01	20.35	0.65	16.95
		1.12	20.86	0.62	16.99
Colour	Mag	0.97	19.64	0.59	17.06
		1.23	21.58	0.95	19.75
NGC 5928		0.95	22.45	0.59	20.00
		1.36	23.40	0.95	20.33
Colour	Mag	0.98	24.14	0.56	20.66
		2.10	24.88	1.01	21.09
NGC 5928		1.08	25.88	0.56	21.23
		2.35	25.88	0.57	22.44
Colour	Mag	1.51	23.58	0.59	18.33
		1.77	24.47	0.62	18.67
NGC 5928		1.99	25.36	0.67	19.07
		2.21	26.18	0.73	19.50
Colour	Mag	1.02	20.77	0.82	19.96
		1.18	21.45	1.07	20.01
NGC 5928		1.47	22.65	0.78	19.93
		1.76	23.82	0.93	20.63
Colour	Mag	1.00	23.11	0.60	20.44
		1.00	23.11	0.66	20.90
NGC 5928		0.72	21.29	1.12	21.56
		0.81	21.85	1.27	22.61
Colour	Mag	0.92	22.51	1.33	23.31
		1.00	23.11	0.92	22.51

Table 7. Fiducial points in the plane: $(m_{F606W} - m_{F814W})$, m_{F606W} .

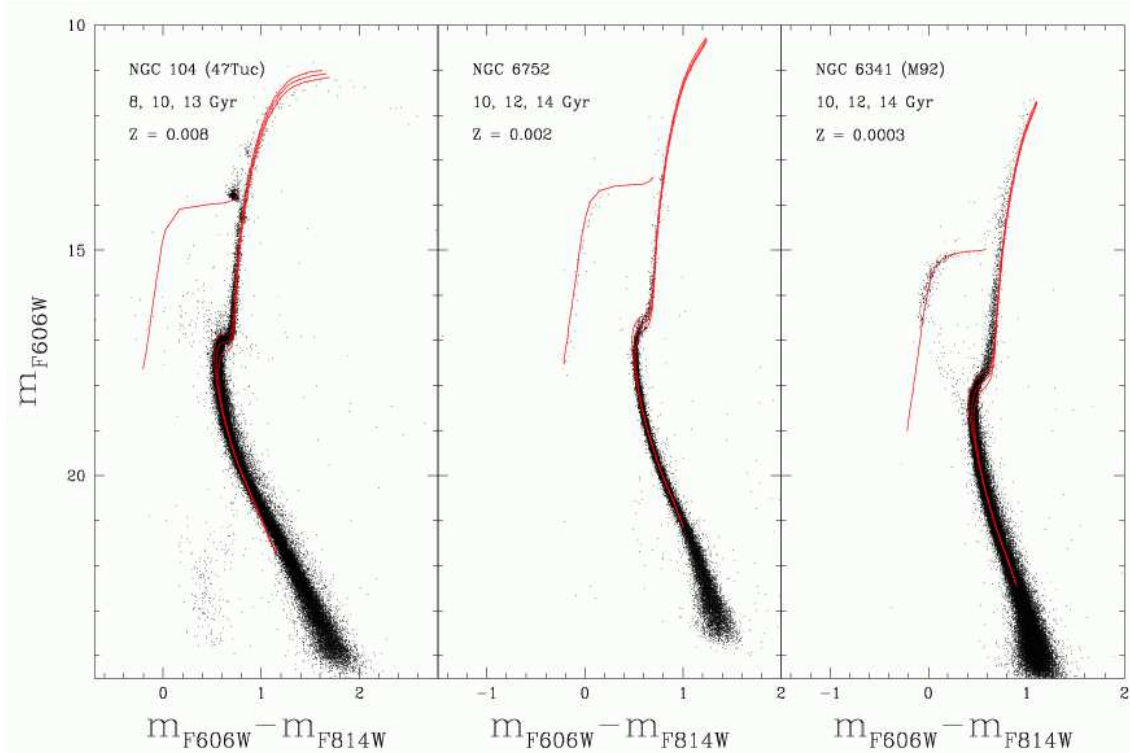


Figure 3. Comparison of three GGCs CMDs (M 92, NGC 6752 and 47 Tuc) with the corresponding isochrones (see text for details).

and the most up to date in-flight transmission curves of the ACS camera. We have named this new in-flight system the *WFC/ACS Vega-mag photometric system*. The proposed calibration is accurate at the level of a few hundredths of a magnitude. We give the basic recipes to calibrate both the observed data and the models,

and present a set of models by Pietrinferni et al. (2004) already transformed into the new ACS Vega-mag system.

Since the primary purpose of this investigation is to make available to the public a complete set of stellar models and isochrones transformed to the ACS Vega-mag system, we have de-

veloped the following web site where all models and isochrones can be retrieved: <http://www.te.astro.it/BASTI/index.php>.

We show CMDs for 5 Galactic globular clusters, spanning a metallicity range $-2.2 < [\text{Fe}/\text{H}] < -0.04$; these CMDs have been obtained from ACS observations, calibrated to the ACS Vega-mag system, and used to test our models. We also give the fiducial points representing their RGB, SGB, and Main Sequence from the red giant branch tip to several magnitudes below the TO. These CMDs and fiducial points will be useful for the study of the old stellar populations in other stellar systems (Brown et al. 2003).

ACKNOWLEDGMENTS

We are very thankful to Marco Sirianni for providing us with the ACS/WFC transmission curves, and also for discussions. We thank the anonymous referee for useful suggestions, James Manner for a careful reading of the manuscript, and Phil James for polishing it. This work has been partially supported by the Agenzia Spaziale Italiana and by the Ministero dell'Istruzione, Università e Ricerca under the program PRIN2003.

REFERENCES

Alexander D. R., Ferguson J. W., 1994, *ApJ*, 437, 879
 Anderson J., King I. R., 2000, *PASP*, 112, 1360
 Angulo C., Arnould M., Rayet M., et al. (NACRE Collaboration), 1999, *Nucl. Phys. A*, 656, 3
 Bahcall J. N., Serenelli A. M., Pinsonneault M., 2004, *ApJ*, submitted, (astro-ph/0403604)
 Bedin L. R., Anderson J., King I. R., Piotto G., 2001 *ApJ*, 560, L75
 Bessell M. S., 1990, *PASP*, 102, 1181
 Bessell M. S., Castelli F., Plez B., 1998, *A&A*, 333, 231
 Böhm-Vitense E., 1958, *Z. Astrophys.*, 46, 108
 Brown T. et al., 2003, *ApJ*, 592, L17
 Carretta E., Gratton R. G., 1997, *A&AS*, 121, 95
 Cassisi S., Salaris M., 1997, *MNRAS*, 285, 593
 Cassisi S., Salaris M., Irwin A. W., 2003, *ApJ*, 588, 862
 Cassisi S., Castellani V., degl'Innocenti S., Weiss A., 1998, *A&AS*, 129, 267
 Castellani V., Chieffi A., Pulone L., Tornambé A., 1985, *ApJ*, 296, 204
 Castelli F., Kurucz R. L., 1994, *A&A* 281, 817
 Castelli F., Kurucz R. L., 2003, Proceed. of IAU Symp. 210, Modelling of Stellar Atmospheres, eds. N. Piskunov et al., poster A20 on the enclosed CD-ROM, (astro-ph/0405087)
 Chaboyer B., 1995, *ApJL*, 444, 9
 Cox J. P., Giuli R. T., 1968, in 'Principles of Stellar Structure', Gordon & Breach, London, Vol. II
 De Marchi G., Sirianni M., Gilliland R., Bohlin R., Pavlosky C., Jee M., Mack J., van der Marel R. & Boffi F. Instrument Science Report ACS 2004-08
 Grboske H. C., DeWitt H. E., Grossman A. S., Cooper M. S., 1973, *ApJ*, 181, 457
 Gratton R. G., Bragaglia A., Carretta E., Clementini G., Desidera S., Grundahl F., Lucatello S., 2003. *A&A*, 408, 529
 Grevesse N., Noels A., 1993, in Origin and Evolution of the Elements, ed. N. Prantzos, E. Vangioni-Flam, M. Cassé (Cambridge: Cambridge Univ. Press), 14
 Haft M., Raffelt G., Weiss A., 1994, *ApJ*, 425, 222
 Holtzman J. A., Burrows C. J., Casertano S., Hester J. J., Trauger J. T., Watson A. M., Worthey G., 1995, *PASP*, 107, 1065
 Krishna-Swamy K. S., 1966, *ApJ*, 145, 174
 Krist J., Instrument Science Report ACS 2003-06
 Kunz R., Fey M., Jaeger M., Mayer A., Hammer J. W., Staudt G., Harissopoulos S., Paradellis T., 2002, *ApJ*, 567, 643
 Iglesias C. A., Rogers F. J., 1996, *ApJ*, 464, 943
 Landolt-Börnstein 1982, Numerical Data and Functional Relationships in Science and Technology, vol.2, Astronomy and Astrophysics
 Mathis J. S., 1990, *ARA&A*, 28, 37
 Momany Y., Cassisi S., Piotto G., Bedin L. R., Ortolani S., Castelli F., Recio-Blanco A., 2003, *A&A*, 407, 303
 Percival S. M., Salaris M., van Wyk F., Kilkenny D., 2002, *ApJ*, 573, 174
 Pietrinferni A., Cassisi S., Salaris M., Castelli F., 2004, *ApJ*, in press, (astro-ph/0405193)
 Potekhin A. Y., 1999, *A&A*, 351, 787
 Reimers D., 1975, *Mem. Soc. R. Sci. Lige*, 8, 369
 Riello M. et al. 2003, *A&A*, 410, 553
 Riess A. & Mack J. Instrument Science Report ACS 2004-006
 Rogers F. J., 2001, *Contrib. Plasma. Phys.*, 41, 179
 Rutledge G. A., Hesser J. E., Stetson P. B. 1997, *PASP*, 109, 907
 Salaris M., Riello M., Cassisi S., Piotto G., 2004, *A&A*, 420, 911
 Sirianni M., De Marchi G., Gilliland R., Bohlin R., Pavlosky C., Mack J., 2002, HST Calibration Workshop 2002, ed. S. Arribas, A. Koekemoer, B. Whitmore (Baltimore: STScI), p. 13
 Sirianni M., Jee M., Ford, H., Illingworth, G., Clampin, M., Hartig, G., De Marchi, G., Gilliland, R., Benitez, N., Blakeslee, J., Mack, J., Martel, A., and McCann W.J. 2004, submitted to *PASP*
 Spergel D. N., Verde L., Peiris H. V. et al., 2003, *ApJS*, 148, 175
 Zinn R., & West M. J., 1984, *ApJS*, 55, 45